communications materials

Article

https://doi.org/10.1038/s43246-024-00526-z

# Anisotropic charge transport at the metallic edge contact of $ReS_2$ field effect transistors



Hyokwang Park[1,3], Myeongjin Lee[1,3], Xinbiao Wang[1,3], Nasir Ali[1], Kenji Watanabe[2], Takashi Taniguchi[2], Euyheon Hwang[1] ✉ & Won Jong Yoo[1] ✉

The in-plane anisotropy of electrical conductance in two-dimensional materials has garnered significant attention due to its potential in emerging device applications, offering an additional dimension to control carrier transport in 2D devices. However, previous research has primarily focused on the anisotropy within electrical channel, neglecting the significant impact of anisotropic electrical contacts of 2D materials. Here, we investigate anisotropic charge transport at the metal contacts of hBN-encapsulated $ReS_2$ using edge-contacted Field Effect Transistors. We observed the marked difference in contact resistance between the *cross-b* and *b* directions, suggesting that charge transport from the metal to $ReS_2$ is more efficient along the *b* direction. This difference in efficiency results in a substantial contact anisotropy, reaching ~70 at 77 K. Our findings indicate that the measured Schottky Barrier Height along the *b* direction is ~35 meV, which is smaller than along the *cross-b* direction. Moreover, the tunneling probability along the *b* direction is two times larger than along the *cross-b* direction. Our results indicate that both Schottky Barrier Height and tunneling amplitude are the primary contributors to the high contact anisotropy of $ReS_2$. This work provides a valuable guideline for understanding how in-plane orientation influences charge transport at metallic contacts in 2D devices.

Since the discovery of monolayer black phosphorus (BP), the interest in anisotropic two-dimensional (2D) materials such as BP, rhenium diselenide ($ReSe_2$) and other transition metal dichalcogenides (TMDs) has increased and the extensive study on anisotropic 2D materials has been conducted, as they introduce an additional degree of freedom to control carrier transport of 2D devices. Among these anisotropic 2D materials, rhenium disulfide ($ReS_2$) stands out as an n-type semiconducting 2D material with a thickness-independent direct band gap and a high on-off ratio[1–7], in addition to its strong in-plane anisotropic electrical[1,2,8] and optical properties[9–13] dependent on the different crystallographic orientations. These unique properties make anisotropic $ReS_2$ highly promising for various future electronic and optoelectronic applications, including tunneling field-effect transistors (FETs), inverters, and photodetectors, capitalizing on its intriguing in-plane anisotropic characteristics[1,3,4,14–17].

Recently, Wang et al. reported the conductance anisotropy controlled by thermionic emission and carrier drift in low-symmetry $ReS_2$ transistors[18]. On the other hand, our group employed the edge contact method to eliminate out-of-plane conductance, so that precise measurement of the orientation-dependent in-plane conductance of the BP channel can be made. As a result, we reported a high anisotropy ratio in channel mobility, ~7.5, for BP FETs[19]. However, we have observed that the contact resistance in 2D TMD-based FETs, such as $ReS_2$, is significantly higher than that in narrow bandgap BP, leading to a pronounced dependence of charge transport anisotropy on the contact resistance, which differs from the behavior seen in BP FETs. There also have been studies to enhance electrical performances of 2D devices by using edge contacts, eg. edge termination of chemical bonds[20–23] and in situ edge cleaning by argon (Ar) ion beam treatment[24,25].

However, previous research works including ones of our research group have reported mainly on the conductance anisotropy in the channel, not the contact resistance anisotropy, particularly with edge contact[8,18,19]. We find that studying the contact resistance anisotropy in 2D FETs with edge contact is very critical for utilizing high anisotropy ratio that can be obtained from future asymmetric orientation-dependent FETs. Also, as the role of

[1]SKKU Advanced Institute of Nano Technology, Sungkyunkwan University, Suwon, Gyeonggi-do 16419, Republic of Korea. [2]National Institute for Materials Science, 1-1 Namiki, Tsukuba 305-0044, Japan. [3]These authors contributed equally: Hyokwang Park, Myeongjin Lee, Xinbiao Wang.
✉e-mail: euyheon@skku.edu; yoowj@skku.edu

contact resistance becomes more significant in nanometer-scale FETs, studying contact anisotropy will become more important to demonstrate the FETs with more design freedom. This aspect has not been adequately explored while the conventional top contact employed in 2D electronic devices involves out-of-plane charge transport at the metal-2D channel interface which cannot be matched to in-plane anisotropic charge transport in the 2D channel, rendering the top contact unable to measure orientation-dependent contact resistance. Consequently, it becomes highly relevant and significant to investigate the influence of anisotropic metal contacts on charge transport using edge-contacted devices.

So, in this work, we present an experimental study on contact anisotropy which refers to the anisotropy ratio of contact resistance obtained from different directions in several device designs, for the first time. Moreover, we applied the edge contact method to implement contact resistance dominant devices in which the contact region is reduced to larger than 100 times. The device structures are devised to eliminate out-of-plane charge transport so as to realize the pristine high contact anisotropy. We prepared the $ReS_2$ encapsulated by hexagonal boron nitride (hBN) via the identification of the orientation of metallic contact edges by performing Raman spectroscopy. We extracted contact resistances along different in-plane directions by varying temperature and gate voltage. Additionally, we conducted experimental measurements of Schottky barrier heights (SBHs) and theoretical calculations of tunneling probabilities to elucidate the mechanisms underlying contact anisotropy in $ReS_2$ FETs. We further present energy band diagrams at the interface formed between metal and $ReS_2$ for the purpose of revealing charge transport mechanisms dependent on contact anisotropy in the $ReS_2$ FETs.

## Results and discussion

### Orientation differentiation and configuration of $ReS_2$

The edge-contacted $ReS_2$ device with four electrodes formed according to the *b* and *cross-b* directions are shown in Fig. 1a. Further, we fabricated edge-contacted $ReS_2$ devices with different designs for the purpose of eliminating possible parasitic current transport arising from the edge front perpendicular to b and cross-b directions with fully trans-etched channel as shown in Supplementary Fig. 1. Figure 1b illustrates the atomic structure of $ReS_2$, which exhibits a distorted 1T structure with Re chains. The chain direction corresponds to the *b* direction, while the direction perpendicular to the *b* direction is referred to as the *cross-b* direction[8]. Generally *a* direction and *b* direction, which has an angle of ~120°, have been used to analyze the anisotropy of $ReS_2$ based on its crystal structure[1]. In this study, however, we compared the transport properties of the *b* and *cross-b* directions instead of the *a* and *b* directions because the largest anisotropy of current is observed along those directions. In Supplementary Fig. 2, we show the direction-dependent currents of $ReS_2$ and find that the largest difference of current occurs between the *b* and *cross-b* directions. Also, as shown in Supplementary Fig. 2, the *cross-b* direction allows clearer contact between the rhenium chain and metal, resulting in a more refined and precise contact compared to *a* direction. Raman spectra of $ReS_2$ encapsulated between top and bottom hBN were measured by rotating the polarizing angle by 15° using a 532 nm laser. Figure 1c presents a polar plot of the normalized Raman intensities of $A_g^7$ as a function of the rotating angle. The normalized Raman intensities of $A_g^7$ exhibit a minimum at 0° and a maximum at 90°, corresponding to the *cross-b* and *b* directions of $ReS_2$, respectively. As shown in Supplementary Fig. 3, the Raman peaks of $A_g^1$, $A_g^6$ and $A_g^7$ for $ReS_2$ are found at 150 $cm^{-1}$, 162 $cm^{-1}$ and 212 $cm^{-1}$, respectively[26]. The *b* and *cross-b* directions are determined by the $A_g^7$ Raman peak of $ReS_2$ as shown in Fig. 1c. Also, $ReS_2$ has the direction which is rotated ~119° from the Re chain direction which is determined by the $A_g^1$ Raman peak of $ReS_2$[9,27]. Although other directions exist in $ReS_2$, we mainly investigate the *b* and *cross-b* directions of $ReS_2$ because the drain current ($I_D$) showed a maximum in the *b* direction and a minimum in the *cross-b* direction based on electrical characterization results of the angle-resolved edge-contacted $ReS_2$ device as shown in Supplementary Fig. 2. The fabrication process of the devices is illustrated in Supplementary Fig. 4. Figure 1d, e shows schematics of edge-contacted devices oriented along the *b* and *cross-b* directions, respectively. Figure 1f shows a cross-sectional high-resolution transmission electron microscopy (HRTEM) image of the contact region of the $ReS_2$ devices with edge contact. The HRTEM image reveals a clean van der Waals interface between hBN and $ReS_2$, demonstrating a high-quality heterostructure stacking. Supplementary Fig. 5 illustrates the analyzed electrical dispersive spectroscopy profile, providing clear evidence of the successful formation of edge-contacted $ReS_2$ FETs and the robust metal contact at the tilted edge of $ReS_2$. Note that our previous paper reported anisotropic channel properties

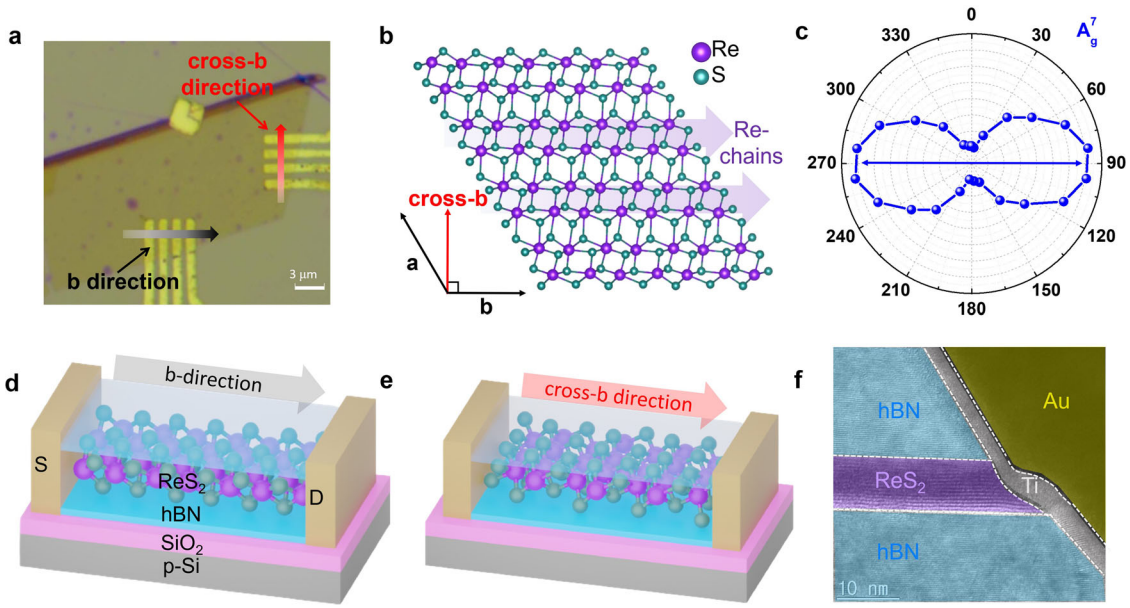


**Fig. 1 | Edge-contacted $ReS_2$ FETs. a** $ReS_2$ crystalline structure with Re chains showing *b* and *cross-b* directions. **b** Polar plot of normalized Raman peak intensities obtained at 212 $cm^{-1}$ which manifests the b direction at the intensity maximum. **c** Optical microscopy image of the edge-contacted $ReS_2$ FET in different directions. **d, e** Schematics of edge-contacted $ReS_2$ FETs along b and cross-b directions. **f** Cross-sectional HRTEM image of the edge-contacted $ReS_2$ consisting of $ReS_2$, hBN, Ti, and Au shown in fake colors.

of BP using edge contact which is able to measure in-plane conductance precisely without out-of-plane conductance[19]. However, we found that not only channel but also contact properties are understood to further influence the anisotropic behavior significantly.

### Elucidating the electrical properties of $ReS_2$ through directional edge contacts

Therefore, we investigated the anisotropy of contact resistance of edge-contacted $ReS_2$ device by performing both 2-point probe (2PP) and 4-point probe (4PP) electrical characterization[28]. Figure 2a, b displays the temperature-dependent 2PP transfer curves obtained from the *b* and *cross-b* directions, respectively, at a drain voltage $V_D$ = 1 V in the temperature range of 77 to 300 K. The drain current increases as temperature increases in both directions, indicating that the device behaves as a typical semiconductor. We extracted contact resistances of edge-contacted $ReS_2$ devices by performing both 2PP and 4PP electrical characterization. Figure 2c shows the contact resistances obtained from the *b* and *cross-b* directions as a function of the gate voltage in the range from −60 to 60 V at 77 and 300 K. Throughout the entire range of gate voltage, the contact resistance along the *cross-b* direction exhibits consistently higher values compared to that along the *b* direction. Furthermore, as the gate voltage is increased, a noticeable reduction in the contact resistances is observed for both directions. Figure 2d presents the contact resistances obtained from the *b* and *cross-b* directions as a function of temperature (from 77 to 300 K) at a fixed gate voltage ($V_G$ = −10 and 60 V). Throughout the entire temperature range, the contact resistance along the *cross-b* direction exhibits a higher value than that along the *b* direction and the resistance in both directions decreases as the temperature increases. This phenomenon can be ascribed to the thermionic emission of charge carriers at elevated temperatures, enabling them to more efficiently overcome the Schottky barrier at the interface between $ReS_2$ and a metal. In Fig. 2e, f, the ratio of contact resistance along *cross-b* direction to that along the *b* direction is shown as a function of gate voltage and temperature, respectively. The anisotropy of contact resistance between *cross-b* and *b* directions increases as both gate voltage and temperature decrease, reaching ~70 at $V_G$ = −30V at 77 K as shown in Fig. 2e. This is related to the carrier transport mechanism at the interface between metal and $ReS_2$. In Supplementary Fig. 6, we show the device structure and corresponding resistance model used to determine the contact anisotropy between *b* and *cross-b* directions. Because our edge-contacted $ReS_2$ devices mainly depend on contact resistance rather than channel resistance, which is relatively consistent as shown in Supplementary Fig. 7, we use contact resistance values in the calculation of contact anisotropy. Also, we fabricated fully trans-etched devices that cover the entire channel width for each direction, as shown in Supplementary Fig. 8. The contact anisotropy of the devices shows the maximum values of ~107 at 300 K and ~225 at 77 K. Supplementary Fig. 9 illustrates the Hall bar structure of edge-contacted $ReS_2$ showing a similar trend with data presented in Fig. 2. Supplementary Fig. 10 illustrates the electrical anisotropy of a fully trans-etched device with uniform width showing clear and depressed contact anisotropy after etching the parasitic leakage current. To figure out the reason that the contact resistance along the *cross-b* direction is larger than that along the *b* direction, we extracted effective SBH along the *b* and *cross-b* directions.

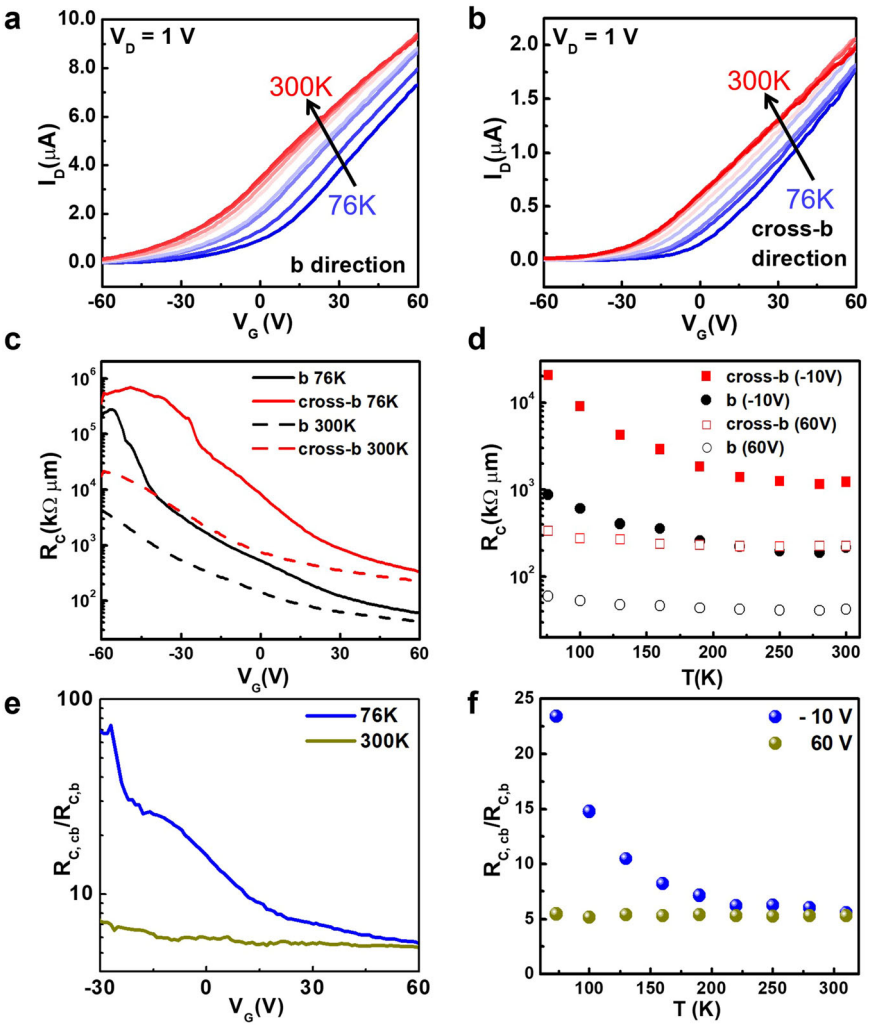


**Fig. 2 | Electrical performance and contact anisotropy of edge-contacted $ReS_2$ FETs. a**, **b** Measured *I*–*V* characteristics by increasing temperature at *b* direction and *cross-b* direction, respectively. The drain voltage is fixed as 1 V. **c**, **d** Measured contact resistance in each direction obtained by 4 Point Probe measurement dependent upon gate voltage and temperature, respectively. **e**, **f** Anisotropy ratios of contact resistance between *b* direction and *cross-b* direction dependent on gate voltage and temperature, respectively.

### Directional Discrepancy in Schottky Barrier Height

Figure 3a, b shows the experimentally extracted effective SBH along the *b* and *cross-b* directions as a function of the gate voltage in the range from −60 V to 60 V. In order to extract the effective SBH, the temperature-dependent transfer curves are used as shown in Supplementary Fig. 11. The SBH is obtained from the thermionic emission equation as shown below[28,29].

$$I_{2D} = WA^{*}_{2D}T^{\frac{3}{2}}\exp\left(-\frac{q\Phi_{SB}}{kT}\right)\exp\left(\frac{qV_{2D}}{kT}\right) \quad (1)$$

$$\Phi_{SB} = \frac{k}{q}\left[-\frac{\Delta\ln(I_{2D}\cdot T^{-\frac{3}{2}})}{\Delta T^{-1}}\right] \quad (2)$$

Here, $W$ is the channel width, $A^{*}_{2D}$ is modified Richardson constant, $q$ is the electron charge, $\Phi_{SB}$ is the Schottky barrier height, $k$ is the Boltzmann constant and $V_{2D}$ is the drain voltage. Equation (2) is derived from Eq. (1) under the assumption that the current might be mainly determined by the Schottky barrier formed at the source under high drain voltage. Figure 3c, d shows the Arrhenius plots which indicate $\ln I_D \cdot T^{-\frac{3}{2}}$ vs. $1000\cdot T^{-1}$ while gate voltage varies from −60 to 60 V. We extracted SBH for a reliable comparison at $V_D = 1$ V from the negative slope of the linear fit to $\ln \ln I_{2D} \cdot T^{-\frac{3}{2}}$ as a function of $q\cdot(kT)^{-1}$. The extracted effective SBH values are $q\Phi_b \sim 35$ meV along the *b* direction and $q\Phi_{cb} \sim 46$ meV along the *cross-b* direction at the flat-band position ($V_G = V_{G0}$). There have been studies reporting values higher than this specific value[30], but there have been no papers reporting about different Schottky barrier heights (SBH) observed along different directions. We note that the thermionic current ratio of *b* direction to cross-*b* direction is given by $e^{\Phi_{cb}/\Phi_b}$, which gives approximately 3.6 times bigger resistivity in the *cross-b* than in the *b* direction. As depicted in Supplementary Fig. 12, we observed that the SBH of our devices barely changed by thickness, while the contact resistance was found to be highly dependent on thickness. It was initially expected that the SBH would remain independent of the gate voltages for $V_G > V_{G0}$. However, the extracted effective SBH decreases gradually with the gate voltage due to the tunneling current through the barrier. As $V_G$ decreases below $V_{G0}$, the effective SBH increases linearly because the majority carrier current is determined by electrons in our samples. In Fig. 3e-h we show the schematic energy band diagrams at the metal-$ReS_2$ interface under different gate voltages. The measured SBH at $V_G = 0$ indicates the barrier height at the thermal equilibrium and the flat band position (i.e., at $V_G = V_{G0}$) indicates the band structure without bending of the conduction band. Similar phenomena may occur in the top contact, but the value of contact anisotropy is significantly lower compared to our edge contact, as shown in Supplementary Fig. 13.

### Directional tunneling barrier thickness and tunneling probability discrepancy

To understand the SBH difference between *b* and *cross-b* directions, we investigate the potential profile at the interface between metal and $ReS_2$ using the density-functional theory (DFT). In Fig. 4a, b, we show the cross-sectional schematics of the contact region between metal and $ReS_2$ along the *b* and the *cross-b* directions, respectively. The condition of the simulation is reaveled in Supplementary Fig. 14. When the orientation of 2D materials changes, the crystal structure of the etched surface also changes. Therefore, the anisotropy of the crystal is closely related to the slope of the etched surface[31]. Due to experimental limitations, this study did not analyze the crystalline structure formed on the contact surface of edge-contacted $ReS_2$ FETs by plasma etching processes. However, according to the referenced literature, there are differences in etching rates depending on the direction of 2D materials, which may lead to differences in the etched crystalline cross-section that are practically impossible to analyze[31]. In this regard, the atomic arrangement of $ReS_2$ along the *b* and *cross-b* directions having different edges is selected for simulation conditions. Along the *b* direction, the metal contacts with both Re and S atoms while it contacts only with sulfur atoms along the *cross-b* direction. These atomic configurations induce the different potential profiles at the interface (see Fig. S14). Overall, we find the higher and wider potential barrier along the *cross-b* direction, i.e., the direct contact of metallic Ti with only sulfur atoms gives rise to the higher and wider Schottky barrier. In Fig. 4c the tunnel barrier width is given as a function of inter-atomic distance at the interface. While the experimentally obtained SBHs are closely related to the potential profiles formed at the interface, the difference of SBH and the barrier width between contact directions plays a role in the observed anisotropy of the contact resistance. Due to the distinct atomic arrangement at the edges along the *b* and *cross-b* directions, not only SBH but also the barrier width is varied in each direction. In Fig. 4d, we show the calculated tunneling probability of electrons through the barrier, which determines the current at low temperatures. The tunneling probability of

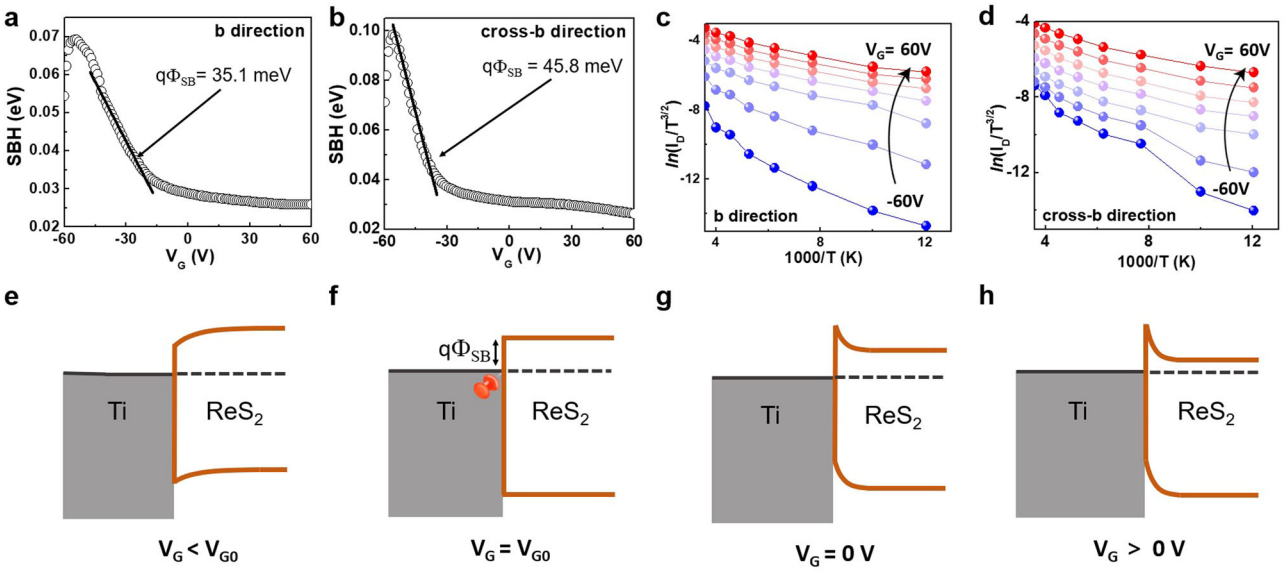


**Fig. 3 | Measured SBHs of $ReS_2$ edge contact FETs. a**, **b** Experimentally extracted SBH at *b* direction and *cross-b* direction, respectively. **c**, **d** Experimentally measured Arrhenius plot of edge-contacted $ReS_2$ along *b* direction and *cross-b* direction, respectively. **e**, **f**, **g**, **h** Band diagram indicating varying SBH at different gate voltages at 0 V, high gate voltage, same at built-in-potential and low gate voltage, respectively.

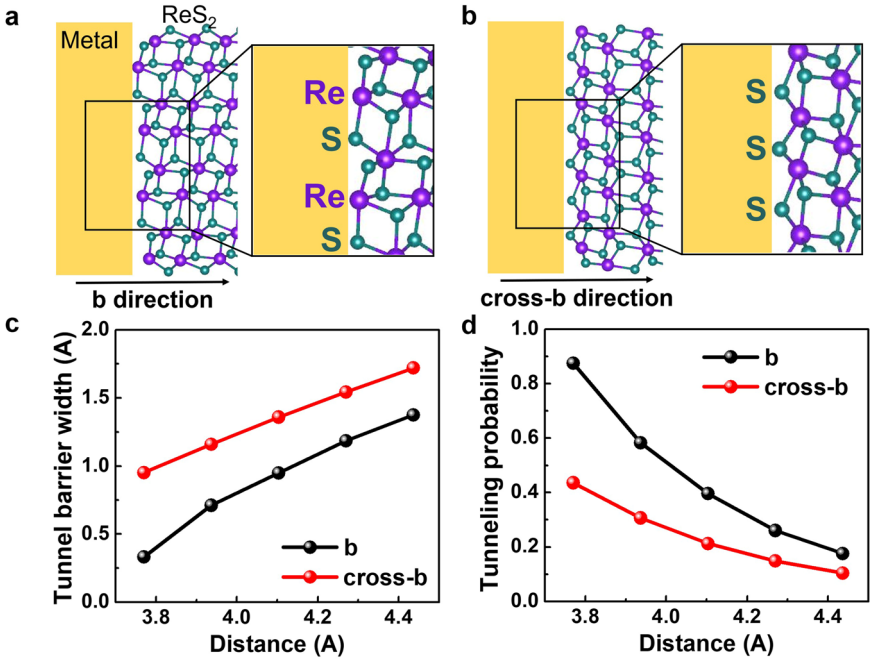


**Fig. 4 | Schematic of metal-$ReS_2$ interfaces and tunneling properties of edge-contacted $ReS_2$ FETs. a, b** Cross sectional schematics of the contact region between metal and $ReS_2$ along *b* direction and *cross-b* direction, respectively. **c, d** Calculated tunnel barrier width and tunneling probability, respectively, showing different distances between Ti and $ReS_2$ in each direction.

carriers can be obtained by [32]

$$P_{TB} = \exp(-\frac{2W_{TB}}{\hbar}\sqrt{2m\Phi_{TB}}) \quad (3)$$

where $W_{TB}$ is the tunneling width, $\hbar$ is the reduced Planck's constant, and $m$ is the mass of the free electron. For interlayer distance from 3.77 Å to 4.44 Å, both tunnel barrier width and tunnel barrier height along the *cross-b* direction are larger than the ones along the *b* direction, which results in the tunneling probability along the *cross-b* direction manifesting a smaller value than along the *b* direction. And tunneling probability ratio between *cross*-b direction and *b* direction increases as the interlayer distance increases. As the distance increases between Ti and $ReS_2$ in the edge contact structure, the tunnel barrier width increases with thicker tunnel barrier width at the *cross-b* direction than the *b* direction. In this regard, the calculated tunneling probability through metal to semiconductor at the *b* direction is higher than at the *cross-b* direction. As reported previously [33], Fermi level pinning, refers to the phenomenon where the Fermi level of a material is fixed at a specific energy level at an interface. Because the Schottky barrier can be formed at the interface although the work function of $ReS_2$ is larger than that of metal. While the difference of SBH along the *b* and *cross-b* directions plays a role in the anisotropy of the transport, the differences in tunneling probability between the *b* and *cross-b* directions seem to give more dominant effects in the highly doped situation. In other words, for high positive gate voltages the tunneling overwhelmingly affects more than the thermionic emission when the charge carriers transfer from metal to $ReS_2$ [19,34]. The electrons injected from metal to $ReS_2$ are more along the *b* direction than along the *cross-b* direction due to tunnel barrier width. Also, as the gate voltage increases, the number of electrons transferred from metal to $ReS_2$ by tunneling mainly increases. For this reason, the anisotropy ratio of contact resistance is more sensitive to the gate voltage than to the temperature.

## Summary

In this study, we have successfully unveiled the underlying mechanisms responsible for contact anisotropy in 2D $ReS_2$. The marked difference in contact resistance between the *cross-b* and *b* directions indicates that charge transport from the metal to $ReS_2$ is much more efficient along the *b* direction. The anisotropy of contact resistance between *cross-b* and *b* directions increases as both gate voltage and temperature decrease, reaching ~70 at $V_G = -30$ V at 77 K. The SBH value measured from the edge-contacted $ReS_2$ device was ~35 meV along the *b* direction and ~46 meV along the *cross-b* direction. Additionally, our calculations of tunneling amplitudes across the edge contact between the metal and $ReS_2$ indicate that the amplitude along the *b* direction is roughly twice as large as that along the *cross-b* direction. These findings collectively support the conclusion that both the SBH and tunneling amplitude play significant roles in contributing to the observed anisotropic contact resistance.

## Methods

### Fabrication of the hBN/$ReS_2$/hBN stack

Hexagonal boron nitride (hBN) and rhenium disulfide ($ReS_2$) were mechanically exfoliated by scotch tape method onto 285 nm thick $SiO_2$/p-Si substrate. Thicknesses of the exfoliated hBN and $ReS_2$ were in the range of 20–40 nm and 10–20 nm, respectively. Thicknesses of these flakes were determined by optical contrast from optical microscopy, and atomic force microscopy. The exfoliated hBN and $ReS_2$ were subjected to a transfer process to form a hBN/$ReS_2$/hBN stack. The hBN and $ReS_2$ were picked up in order by using polycarbonate (PC) at 353–393 K. The hBN/$ReS_2$ stack was dropped down on the exfoliated hBN at 503 K. Residues formed by PC were removed by chloroform.

### Fabrication of the $ReS_2$ edge-contacted device

Angle-resolved Raman measurements on hBN/$ReS_2$/hBN heterostructure were performed to identify the b and cross-b directions of $ReS_2$ using a polarized micro-Raman system equipped with a 532 nm laser with a spot size of 1 μm and a power of 100 mW, and a polarizer. Poly(methylmethacrylate) (PMMA) A6 950 as electron beam resists was applied by spin coating at 4000 rpm for 60 s on the wafer with hBN/$ReS_2$/hBN stack. It was hardened at 180 °C for 90 s. Metal patterns were defined by using electron beam lithography (EBL; JEOL JSM-7001F and Raith ELPHY Plus & Quantum). Electron beam resists were developed by putting in a solution consisting of isopropyl alcohol and deionized water (3:1). To completely remove PC and PMMA residues remaining after the development, UV ozone treatment was carried out for 90 s. The hBN/$ReS_2$/hBN stack was etched by inductively coupled plasma (ICP) at the following processing conditions: ICP power of 20 W, working pressure of 20 mTorr, $SF_6$ and $O_2$ gas flow of 10 and 30 sccm, respectively,

and time of 60 s. 5 nm Ti/80 nm Au were deposited by an electron beam evaporator (Korea Vacuum, KVE-E2000). The lift-off process was carried out in acetone for 1 h after metal deposition.

### Electrical and TEM measurement

The electrical measurements of the fabricated devices were performed by the semiconductor parameter analyzer (Agilent 4155C) and the probe station (MSTECH MST-1000B M6VC) with a vacuum level of 10 mTorr. To analyze $ReS_2$ and metal/$ReS_2$ interfaces, HRTEM was performed. A small region of the fabricated devices including the contact was isolated by focused ion beam milling and was moved to a TEM grid for cross-sectional HRTEM and scanning TEM.

### Calculation methods

To explore the SBH difference between the *b* direction and *cross-b* direction, the density-functional theory (DFT) is studied, using the plane-wave pseudopotential approach according to the Cambridge Sequential Total Energy Package (CASTEP)[35]. The study on the exchange-correlation function of $ReS_2$ is described by the generalized gradient approximation of Perdew, Burke, and Ernzerhof parameterization (PBE)[36]. The electronic wave functions were obtained by using a density-mixing minimization method for self-consistent field calculation. The van der Waals interactions were taken into account by using the DFT + D method by means of Tkatchenko and Scheffler (TS) corrections to PBE[37]. Also, we consider non-self-consistent dipole correction in the calculation process with the setting of the vacuum of about 25 Å spaces to avoid the neighboring layers' interaction in the periodic slabs. The valence electrons which form a chemical bond and define the general properties of atoms, were treated by wave functions with the following electronic configurations: Re $5s^2$ $5p^6$ $5d^5$ $6s^2$; Ti $3s^2$ $3p^6$ $3d^2$ $4s^2$ and S $3s^2$ $3p^4$. The ionic core was described by the Vanderbilt ultrasoft pseudopotential[38]. A plane-wave cut-off energy was chosen at 310 eV. The $2 \times 2 \times 1$ and $2 \times 3 \times 1$ Monkhorst-Pack k-mesh were used for *cross-b* supercell and *b* supercell, respectively [39]. For $ReS_2$/Ti heterostructures, there are two different configurations considered, Ti(100) for contact along *cross-b* direction of $ReS_2$ and Ti(001) for contact along *b* direction of $ReS_2$. Lattice mismatch is less than 3% for both structures. The structural relaxation of the geometries, due to the Hellmann–Feynman forces, was performed within the Broyden, Fletcher, Goldfarb, and Shannon (BFGS) method[40]. The optimization of the studied models was performed until the following convergence criteria were reached: the tolerance of the electronic total energy convergence was $10^{-6}$ eV per atom, the maximum displacement 0.001 angstrom, the maximum force 0.03 eV/angstrom, and the maximum pressure 0.05 GPa.

## Data availability

All relevant data are available from the authors.

## Code availability

The DFT code used in this study was available from the Cambridge Sequential Total Energy Package (CASTEP).

Received: 18 January 2024; Accepted: 21 May 2024;
Published online: 28 May 2024

## References

1. Liu, E. et al. Integrated digital inverters based on two-dimensional anisotropic $ReS_2$ field-effect transistors. *Nat. Commun.* **6**, 6991 (2015).
2. Lin, Y. et al. Single-layer $ReS_2$: two-dimensional semiconductor with tunable in-plane anisotropy. *ACS Nano* **9**, 11249–11257 (2015).
3. Mohammed, O. B. et al. $ReS_2$-based interlayer tunnel field effect transistor. *J. Appl. Phys.* **122**, 245701 (2017).
4. Shim, J. et al. High-performance 2D rhenium disulfide ($ReS_2$) transistors and photodetectors by oxygen plasma treatment. *Adv. Mater.* **28**, 6985–6992 (2016).
5. Xu, K. et al. Sulfur vacancy activated field-effect transistors based on $ReS_2$ nanosheets. *Nanoscale* **7**, 15757–15762 (2015).
6. Corbet, C. M. et al. Field effect transistors with current saturation and voltage gain in ultrathin $ReS_2$. *ACS Nano* **9**, 363–370 (2015).
7. Liu, F. et al. Highly sensitive detection of polarized light using anisotropic 2D $ReS_2$. *Adv. Funct. Mater.* **26**, 1169–1177 (2016).
8. Wang, R. et al. The mechanism of the modulation of electronic anisotropy in two-dimensional $ReS_2$. *Nanoscale* **12**, 8915–8921 (2020).
9. Chenet, D. A. et al. In-plane anisotropy in mono- and few-layer $ReS_2$ probed by Raman spectroscopy and scanning transmission electron microscopy. *Nano Lett.* **15**, 5667–5672 (2015).
10. Yu, J. et al. Tunable anisotropy in $ReS_2$ flakes achieved by $Ar^+$ ion bombardment probed by polarized Raman spectroscopy. *Appl. Phys. Lett.* **119**, 053104 (2021).
11. Yu, J. et al. Anisotropy study of phonon modes in $ReS_2$ flakes by polarized temperature-dependent Raman spectroscopy. *Chem. Phys. Lett.* **810**, 140132 (2023).
12. Wen, T. et al. Analyzing anisotropy in 2D rhenium disulfide using dichromatic polarized reflectance. *Small* **18**, 2108028 (2022).
13. Sim, S. et al. Ultrafast quantum beats of anisotropic excitons in atomically thin $ReS_2$. *Nat. Commun.* **9**, 351 (2018).
14. Zhang, E. et al. $ReS_2$-based field-effect transistors and photodetectors. *Adv. Funct. Mater.* **25**, 4076–4082 (2015).
15. Liu, E. et al. High responsivity phototransistors based on few-layer $ReS_2$ for weak signal detection. *Adv. Funct. Mater.* **26**, 1938–1944 (2016).
16. Tai, X. et al. High-performance $ReS_2$ photodetectors enhanced by a ferroelectric field and strain field. *RSC Adv.* **12**, 4939–4945 (2022).
17. Najmzadeh, M., Ko, C., Wu, K., Tongay, S. & Wu, J. Multilayer $ReS_2$ lateral P-N homojunction for photoemission and photodetection. *Appl. Phys. Express* **9**, 055201 (2016).
18. Wang, Z. et al. Comprehensive modulation of conductance anisotropy in low-symmetry $ReS_2$ transistors. *Phys. Rev. Appl.* **17**, 044017 (2022).
19. Lee, M. et al. Ultrahigh anisotropic transport properties of black phosphorus field effect transistors realized by edge contact. *Adv. Electron. Mater.* **8**, 2100988 (2022).
20. Parto, K. et al. One-dimensional edge contacts to two-dimensional transition-metal dichalcogenides: uncovering the role of schottky-barrier anisotropy in charge transport across $MoS_2$/metal interfaces. *Phys. Rev. Appl.* **15**, 064068 (2021).
21. Houssa, M. et al. Contact resistance at graphene/$MoS_2$ lateral heterostructures. *Appl. Phys. Lett.* **114**, 163101 (2019).
22. Gao, Q. & Guo, J. Role of chemical termination in edge contact to graphene. *APL Mater.* **2**, 056105 (2014).
23. Saha, D. & Mahapatra, S. Anisotropic transport in 1T′ monolayer $MoS_2$ and its metal interfaces. *Phys. Chem. Chem. Phys.* **19**, 10453–10461 (2017).
24. Cheng, Z. et al. Immunity to contact scaling in $MoS_2$ transistors using in situ edge contacts. *Nano Lett.* **19**, 5077–5085 (2017).
25. Abuzaid, H., Cheng, Z., Li, G., Cao, L. & Franklin, A. D. Unanticipated polarity shift in edge-contacted tungsten-based 2D transition metal dichalcogenide transistors. *IEEE Electron Dev. Lett.* **42**, 1563–1566 (2021).
26. McCreary, A. et al. Intricate resonant raman response in anisotropic $ReS_2$. *Nano Lett.* **17**, 5897–5907 (2017).
27. Choi, Y. et al. Complete determination of the crystallographic orientation of $ReX_2$ (X = S, Se) by polarized Raman spectroscopy. *Nanoscale Horiz.* **5**, 308–315 (2020).
28. Mitta, S. B. et al. Electrical characterization of 2D materials-based field-effect transistors. *2D Mater.* **8**, 012002 (2021).
29. Kim, C. et al. Fermi level pinning at electrical metal contacts of monolayer molybdenum dichalcogenides. *ACS Nano* **11**, 1588–1596 (2017).

30. Intonti, K. et al. Temperature-dependent conduction and photoresponse in few-layer $ReS_2$. *ACS Appl. Mater. Interfaces* **15**, 50302–50311 (2023).
31. Danielsen, D. R. et al. Super-resolution nanolithography of two-dimensional materials by anisotropic etching. *ACS Appl. Mater. Interfaces* **13**, 41886–41894 (2021).
32. Merzbacher, E. Quantum Mechanics, 3rd ed. (Wiley: New York, 1997).
33. Liu, X., Choi, M. S., Hwang, E., Yoo, W. J. & Sun, J. Fermi level pinning dependent 2D semiconductor devices: challenges and prospects. *Adv. Mater.* **34**, 2108425 (2022).
34. Ngo, T. D., Choi, M. S., Lee, M., Ali, F. & Yoo, W. J. Anomalously persistent P-type behavior of $WSe_2$ field-effect transistors by oxidized edge-induced fermi-level pinning. *J. Mater. Chem. C* **10**, 846–853 (2022).
35. Segall, M. D. et al. *J. Phys. Condens. Mater.* **14**, 2717 (2022).
36. Perdew, J. P., Burke, K. & Ernzerhof, M. Generalized gradient approximation made simple. *Phys. Rev. Lett.* **77**, 3865 (1996).
37. Tkatchenko, A. & Scheffler, M. Accurate molecular van der Waals interactions from ground-state electron density and free-atom reference data. *Phys. Rev. Lett.* **102**, 073005 (2009).
38. Vanderbilt, D. Soft self-consistent pseudopotentials in a generalized eigenvalue formalism. *Phys. Rev. B.* **41**, 7892 (1990).
39. Monkhorst, H. J. & Pack, J. D. Special points for Brillouin-zone integrations. *Phys. Rev. B.* **13**, 5188 (1976).
40. Zhu, W. & Xiao, H. Ab initio study of electronic structure and optical properties of heavy-metal azides: $TlN_3$, $AgN_3$, and $CuN_3$. *Comput. Chem.* **29**, 176 (2008).

## Acknowledgements

H. Park, M. Lee, and X. Wang contributed equally to this work. This work was supported by the National Research Foundation of Korea (RS-2024-00346656 and 2021R1A2C1012176). It was also supported by the Ministry of Trade, Industry and Energy (20022369).

## Author contributions

H.P., M.L., X.W., E.H., W.J.Y. conceived of the research project. E.H. and W.J.Y. supervised the experiment and wrote the manuscript. H.P., M.L. fabricated sandwiched $ReS_2$ structure and characterized the devices electrically and optically. X.W. performed a simulation on contact between $ReS_2$ and Ti. K.W. and T.T. provided hBN samples used in the work. N.A. assisted device measurement and analysis.

## Competing interests

The authors declare no competing interests.

## Additional information

**Supplementary information** The online version contains supplementary material available at https://doi.org/10.1038/s43246-024-00526-z.

**Correspondence** and requests for materials should be addressed to Euyheon Hwang or Won Jong Yoo.

**Peer review information** *Communications Materials thanks* Antonio Di Bartolomeo and the other, anonymous, reviewer(s) for their contribution to the peer review of this work. Primary Handling Editor: Aldo Isidori. A peer review file is available.